Energy 143 (2018) 666–681

Contents lists available at ScienceDirect

Energy

journal homepage: www.elsevier.com/locate/energy

Direct route from ethanol to pure hydrogen through autothermal reforming in a membrane reactor: Experimental demonstration, reactor modelling and design

V. Spallina [a, c, *], G. Matturro [a], C. Ruocco [b], E. Meloni [b], V. Palma [b], E. Fernandez [c], J. Melendez [c, d], A.D. Pacheco Tanaka [c], J.L. Viviente Sole [c], M. van Sint Annaland [a], F. Gallucci [a, **]

[a] Chemical Process Intensification, Department of Chemical Engineering and Chemistry, Eindhoven University of Technology, Eindhoven, The Netherlands
[b] Processes and Catalysis for Energy and Environment Depollution, Industrial Engineering Department, University of Salerno, Fisciano, Italy
[c] Membrane Technology Group, Energy and Environment Division, Tecnalia, San Sebastián-Donostia, Spain
[d] Chemical Engineering and Environmental Department, University of the Basque Country UPV/EHU, Bilbao, Spain

ARTICLE INFO

Article history:
Received 11 April 2017
Received in revised form
19 September 2017
Accepted 5 November 2017
Available online 8 November 2017

Keywords:
Ethanol reforming
Palladium membranes
Membrane reactor
Hydrogen production
Experimental demonstration
Modelling

ABSTRACT

This work reports the integration of thin (~3–4 μm thick) Pd-based membranes for H_2 separation in a fluidized bed catalytic reactor for ethanol auto-thermal reforming. The performance of a fluidized bed membrane reactor has been investigated from an experimental and numerical point of view. The demonstration of the technology has been carried out over 50 h under reactive conditions using 5 thin Pd-based alumina-supported membranes and a 3 wt%Pt-10 wt%Ni catalyst deposited on a mixed CeO_2/SiO_2 support. The results have confirmed the feasibility of the concept, in particular the capacity to reach a hydrogen recovery factor up to 70%, while the operation at different fluidization regimes, oxygen-to-ethanol and steam-to-ethanol ratios, feed pressures and reactor temperatures have been studied. The most critical part of the system is the sealing of the membranes, where most of the gas leakage was detected. A fluidized bed membrane reactor model for ethanol reforming has been developed and validated with the obtained experimental results. The model has been subsequently used to design a small reactor unit for domestic use, showing that 0.45 m^2 membrane area is needed to produce the amount of H_2 required for a 5 kW_e PEM fuel-cell based micro-CHP system.

1. Introduction

H_2 represents an important product for the chemical industry [1], and its demand is constantly increasing, also due to its potential use as automotive fuel and energy carrier [2]. Nowadays, fossil fuels (and mostly natural gas) are used for the production of more than 95% of the global H_2. Currently, H_2 is almost entirely used as feedstock within the refining and chemical industries to convert raw materials into higher value chemicals (e.g. NH_3, CH_3OH) or refinery hydro-treating processes [3]. In addition, H_2 represents the most important energy carrier for the future and can play an important role in reducing the anthropogenic greenhouse gas emissions. Recently, fuel cells have been developed and launched to the market and a lot of research is ongoing to investigate and develop the technologies for the transition towards H_2 [4]. Among the various renewable feedstock alternatives, ethanol (EtOH) is considered as an attractive feedstock due to its relatively high hydrogen content, abundant availability, non-toxicity, storage or handling ease and safety [5–7]. Moreover, the ethanol can be produced renewably by biomass sources (agricultural wastes, forestry residuals or organic municipal wastes, etc.), also called bio-ethanol, and is mixed with water (about 15% on weight basis of EtOH [8]). The ethanol-to-hydrogen conversion is normally attained by ethanol reforming reactions that can be classified in: i) steam reforming (ESR) and ii) auto-thermal reforming (EAR) in the

* Corresponding author. Chemical Process Intensification, Department of Chemical Engineering and Chemistry, Eindhoven University of Technology, Eindhoven, The Netherlands.
** Corresponding author. Chemical Process Intensification, Department of Chemical Engineering and Chemistry, Eindhoven University of Technology, Eindhoven, The Netherlands.
E-mail addresses: v.spallina@tue.nl (V. Spallina), f.gallucci@tue.nl (F. Gallucci).

https://doi.org/10.1016/j.energy.2017.11.031
0360-5442/

presence of an oxidant (air or oxygen). Sun et al. [9] have conducted a thermodynamic study on ethanol reforming comparing steam reforming, auto-thermal reforming and partial oxidation and they have found the optimal conditions at 900 K, with steam-to-ethanol equal to 6 and oxygen-to-ethanol equal to 0.25. Similarly, de Avila et al. [10] presented their study including also the dry reforming and they found a mismatch in the maximum H_2 mol fraction (around 773–873 K) and H_2 yield (when the temperature is higher than 1123 K).

The reaction pathways for ethanol reforming include several possible reactions which are influenced by the catalyst and the operating conditions used in system [5,11,12]. Different supported/unsupported catalysts have been proposed in the literature for the ESR reaction which have been summarized in a recent review from Hou et al. [11], where both noble metal catalysts (Rh, Ru, Pt, Pd) operated in the range of 650–750 °C with a steam-to-ethanol ratio (H_2O/EtOH) of 1–3 (and also O_2 co-feeding) and transition metals (especially Ni and Co) operated at a lower temperature (350–650 °C) with a higher H_2O/EtOH ratio (up to 10 on a molar basis) have been considered. However, the addition of small quantities of noble metals to transition metals-based catalysts was shown to improve the ethanol conversion and H_2 yield even at low temperatures and/or steam-to-carbon ratios [13]. As support material, alumina (Al_2O_3) has been widely studied because of its strong thermal and mechanical stability, despite the fact that it may allow the formation of C_2H_4 which is a precursor for coke formation. In general, supports such as CeO_2 and mixed oxides systems have shown to be highly favourable in terms of EtOH conversion and H_2 selectivity reducing the sintering effect because of metal dispersion through the support [13,14]. As a result, the application of the high surface area of a CeO_2/SiO_2 mixed system has shown improved catalytic stability with respect to SiO_2 free samples [15].

H_2 production from ethanol is normally carried out via multiple steps of conversion and separation processes [12,16]. The reforming is carried out at 750–800 °C, where the ethanol is decomposed in other gaseous species (CH_4, CO, H_2) as indicated in Equation (1), making the conversion of ethanol into H_2 thermodynamically limited. In the ethanol auto-thermal reforming (EAR), the presence of oxygen reduces the H_2 selectivity, however, no external furnace is required to supply the required heat of reaction for the highly endothermic ESR. Due to the thermodynamic equilibria, large quantities of CO are produced. The main reactions occurring in the EAR reactor are:

$$C_2H_5OH \rightarrow H_2 + CO + CH_4 \quad \Delta H_0^{298K} = 51.3 kJ/mol \tag{1}$$

$$CH_4 + H_2O \leftrightarrow 3H_2 + CO \quad \Delta H_0^{298K} = 206.2 kJ/mol \tag{2}$$

$$CH_4 + 0.5O_2 \leftrightarrow 2H_2 + CO \quad \Delta H_0^{298K} = -38 kJ/mol \tag{3}$$

$$CO + H_2O \leftrightarrow H_2 + CO_2 \quad \Delta H_0^{298K} = -41.2 kJ/mol \tag{4}$$

In the complete process, the H_2 yield can be enhanced by employing additional water-gas-shift (WGS) reactors, producing H_2 and CO_2 while reducing the CO content below 1–0.5 vol% In some processes, the presence of CO in the H_2-rich stream acts as a poison for the materials of the downstream units (e.g. fuel cells, NH_3 synthesis, etc.). In these cases, a further purification step is required to obtain high purity H_2, and usually a methanation reactor is considered to further decrease the CO content to below 10 ppm converting CO into CH_4 [17]. Alternatively, pressure swing absorption (PSA), cryogenic distillation, or membrane technology can be used to produce high purity H_2 (>99.99%).

The overall H_2 yield of ethanol reforming is usually about 4.3 mol_{H2}/mol_{EtOH} [16]. However, in case pure H_2 is required, the application of PSA (with an H_2 separation factor of about 80%) leads to an overall efficiency (based on the LHV) of 65% (<3.5 mol_{H2}/mol_{EtOH}).

Recently, several studies have been devoted to the integration of ethanol reforming and H_2 separation using Pd-based membranes [18–21] also including the application of those for the transport sector [22]. Due to the high efficiency and high purity achieved, Pd-based membrane reactor are particularly suitable to be integrated with PEM fuel cells in domestic unit to provide heat and electricity higher than 2 kW [23]. Pd-based membranes are inorganic membranes in which H_2 permeates selectively from the feed/retentate to the permeate side. Pd-based membranes are normally alloyed with other metals (Cu, Ag, Au, etc.) to enhance the performance and the tolerance to embrittlement and poisonous gases (i.e. H_2S) and generally are thin films supported on metallic or ceramic supports in order to enhance the mechanical resistance while achieving high fluxes [24–28]. The retentate side is normally reach in CO_2 and H_2 (<15% vol.), therefore the recovery of fuel species is essential to increases the efficiency of the entire system using a catalytic combustor [29]. Membrane reactors represent a convenient solution to integrate reaction and separation in a single process with several advantages: i) the chemical equilibrium is shifted towards the products and therefore no other conversion units are required, ii) the cost of materials can be reduced by operating at lower temperatures, iii) the H_2 separation and purification is carried out in-situ, iv) the membrane reactor can be integrated in small and medium scale plant. So far, several different processes have been proposed to integrate Pd membranes for H_2 production differing in reactor configuration and/or plant design [26,30,31]. Also membrane reactors for EtOH reforming have been extensively studied. Borgognoni et al. [19] have tested a CH_4/EtOH co-feeding unit in which the reforming is carried out at 750 °C and the H_2 separation is carried out in a downstream membrane separator in which the 70% of the total amount of produced H_2 was recovered at 500 kPa. Basile et al. [20] have tested a packed bed membrane reactor using different H_2O/EtOH ratios (ranging from 3 to 9) at 1.3 bar in the range of 300–400 °C and a Ru-based catalyst supported on Al_2O_3; in this work the total hydrogen recovery factor (HRF) was between 10% and 56% depending on the temperature and the H_2O/EtOH ratio used. Gallucci et al. [32] have proposed a fluidized bed membrane reactor for ethanol reforming in which part of the H_2 is consumed in a dedicated membrane which uses air as sweep gas, so that the combustion provides the heat of reaction for the ethanol reforming while CO_2 capture was integrated: about 15% of the total membrane area is required for combustion to achieve autothermal operation and the maximum CO_2 selectivity was reached at 700 °C due to the higher permeation rate of the membrane at higher temperatures. The use of a fluidized bed reactor improves the temperature control of the system avoiding the possible formation of hotspots, as well as the presence of low temperature zones which may damage the Pd-based membranes because of embrittlement. De Falco [33] has investigated an ethanol membrane reformer integrated with a polymeric electrolyte membrane fuel cell for automotive vehicles, delivering an optimized design of a 0.2 m^3 reactor with 4 membranes (0.285 m^2 of membrane area) operated at 400 °C for the production of 64 $NL \cdot min^{-1}$ of H_2 to work in a PEM fuel cell of 4 kW_e. Foresti and Manzolini [16] have performed a thermodynamic analysis for a micro combined heat and power generation unit (μCHP) in which a fluidized bed membrane reactor is used for ethanol auto-thermal reforming and pure H_2 separation integrated with a 5 kW_e PEM fuel cell to generate heat and electricity for domestic off-grid applications. In their work, the authors have compared different membrane reactor configurations (with and without sweep gas) at 500–550 °C varying the pressure (6–16 bar)

and the composition (H_2O/EtOH from 3 to 4.2) resulting in an optimal system performance (higher than 40% of electrical efficiency compared to 33.1% of the conventional case) at 12 bar and a H_2O/EtOH ratio equal to 3.6 and 0.4 m^2 of membrane area. In case of H_2 separation without sweep gas, the optimal performance that could be achieved at 6 bar and 0.3 bar at the permeate side required 0.3 m^2 membrane area (40.3% based on Ethanol lower heating value). Hedayati et al. [21] have compared the experiments and modelling of a dynamic unit to produce H_2 for fuel cell and they found that the changes in the fuel flow rate responds much faster than the electric part. Recently, Arratibel et al. [34] have summarized the operating conditions and performance of different methane and ethanol reforming membrane reactor for pure H_2 production that have been tested and presented.

In the present paper, a fluidized bed membrane reactor (FBMR) has been tested for ESR and EAR and evaluated from an experimental and numerical point of view. The catalyst material used is 3 wt%Pt-10 wt%Ni deposited onto a mixed CeO_2/SiO_2 support to increase the stability of the catalyst as presented in a previous work [14]. Five ultra-thin ceramic-supported Pd-Ag membranes (4 μm thickness) of 120–160 mm length and 10 mm of external diameter have been sealed and integrated in a lab-scale fluidized bed (previously used to demonstrate a WGS membrane reactor [30]) and tested under reactive conditions. The proof-of-concept has been achieved for different operating conditions. A two-phase phenomenological model for the fluidized bed reactor has been validated with the experimental results and subsequently used for the design of a commercial scale unit.

2. Description of the technology

The schematic representation of a fluidized bed membrane reactor is shown in Fig. 1. The inlet gases, EtOH/H_2O/air, are fed to the bottom part of the reactor through a 40 micron porous plate distributor. All the EtOH is partly oxidized with O_2 and decomposed into other gases (reaction (1)), while the produced CH_4 and CO start to react with H_2O (reactions (2–4)). The supported Pd-Ag membrane tubes are immersed inside the catalyst bed to extract the hydrogen from the reaction zone and enhance the methane reforming and water gas shift reactions. The pressure drop over the bed is negligible, while mass and heat transfer coefficients are higher due to the vigorous solids mixing resulting in a virtually uniform temperature throughout the reactor.

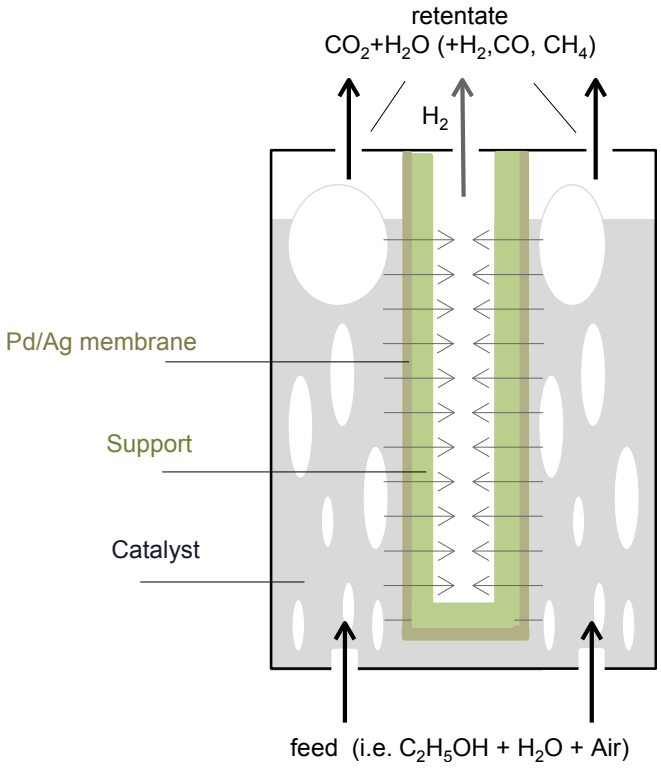

Fig. 1. Schematic layout of a fluidized bed membrane reactor.

The presence of the membranes can improve the bubble-to-emulsion mass transfer rate, since the membranes act as internals in the granular suspension promoting bubble breakage [35]. Due to the gas extraction through the membranes, the solids circulation pattern may be modified compared to the conventional fluidized bed reactor, since densified zones may be formed close to the membranes [36,37].

The integration of catalyst and membranes has been carried out at two different scales: in the first part, a single tube membrane reactor has been used to carry out permeation tests using different reactor layouts (empty, fluidized and packed bed configurations) to verify the validity of the kinetic model proposed in Ruocco et al. [14]. Subsequently, 5 membranes have been sealed and used in a larger prototype, which has been operated close to industrial operating conditions.

2.1. Catalyst preparation

The CeO_2/SiO_2 support material was prepared by adding calcined (at 600 °C for 3 h, heating rate of 10 °C min^{-1}) silica gel (particle size distribution 150–250 μm, supplied by Sigma-Aldrich) to an aqueous solution of $Ce(NO_3)_3 \cdot 6H_2O$ (Strem Chemicals). The CeO_2/SiO_2 weight ratio, previously optimized [15], was fixed at 30%. Impregnation was carried out at 80 °C for 2 h on a heating and stirring plate. Then, the support was filtered by means of a Buchner funnel, dried overnight at 120 °C and calcined as reported above for the bare silica. Ni (10 wt%) and Pt (3 wt%) metal loadings refer to the total ceria mass were sequentially added to the support, starting from $Ni(NO_3)_3 \cdot 6H_2O$ and $PtCl_4$ (Strem Chemicals) as salt precursors, respectively.

BET specific surface areas and porosity of the support as well as the catalyst were determined from the absorption isotherms at 77 K, acquired by means of a ThermoScientific Surfer. Structural properties were characterized by powder X-ray diffraction (XRD) using a D-8 Advance Bruker WAXRD diffractometer under a CuKα radiation of 1.5406 Å. XRD spectra allowed the calculation of average crystallite size by means of Scherrer equation. H_2 Temperature Programmed Reduction (TPR) measurements were carried out in situ in the laboratory apparatus previously described [15]. The temperature was increased to 600 °C (heating rate of 10 °C/min) and held for 1 h under 5%H_2 in N_2 (500 $Ncm^3 \cdot min^{-1}$ of total flow rate). The support and catalysts were prepared and characterized (XRD and TPR analysis) in the Proceed laboratories of the University of Salerno.

2.2. Membrane preparation

Alumina asymmetric tubes with a 10 mm outside diameter were used as membrane supports. Pd-Ag thin layers were deposited onto the alumina tubes using the simultaneous (Pd and Ag) electroless plating technique reported in Pacheco Tanaka et al. [38]. After the plating step, the membrane layers were annealed at 550 °C with a H_2-N_2 gas mixture. The final membranes are approximately 140–230 mm in length and with a Pd-Ag thickness of around 3–4 μm (Fig. 2).

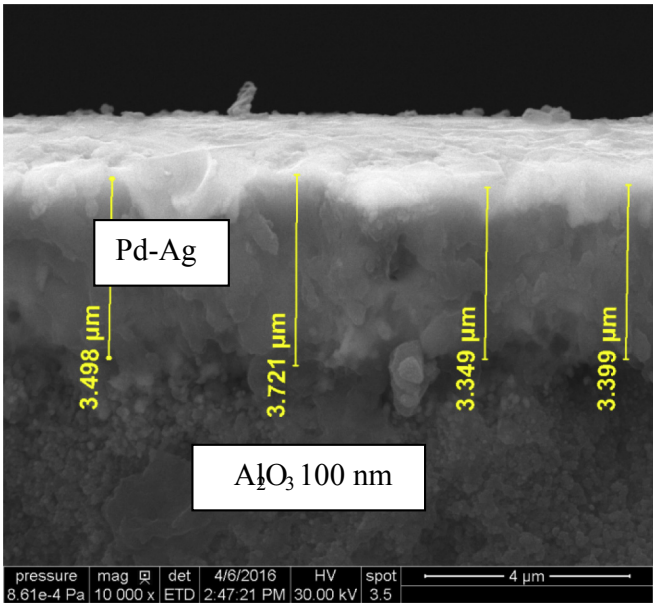

Fig. 2. Cross-section SEM image of a Pd-Ag membrane layer deposited onto an Al_2O_3 asymmetric porous tube (100 nm pore size, 10/4 mm OD/ID).

2.3. Reactor design and test rig

Two different reactors have been used in this work. The first reactor is a single tube membrane reactor (Fig. 3a) which has been used for the permeation tests and the validation of the kinetic modelling by feeding a mixture of CH_4, CO and H_2 and H_2O under fluidization conditions. The membrane (named E275) is 5.5 cm in length and has an external diameter of 10 mm (Fig. 3b). The sealing method has been proposed by Chen et al. [39] in which graphite ferrules, instead of metal ferrules are used. The same method has been successfully used for a long-term test under reactive conditions [24,30,40]. The reactor is placed in an electrically heated oven in order to have a constant temperature along the entire reactor. A second membrane (E273) of 10.4 mm (ID) and 109.8 cm length was also used for the permeation test using respectively the empty bed, packed bed and fluidized bed configurations.

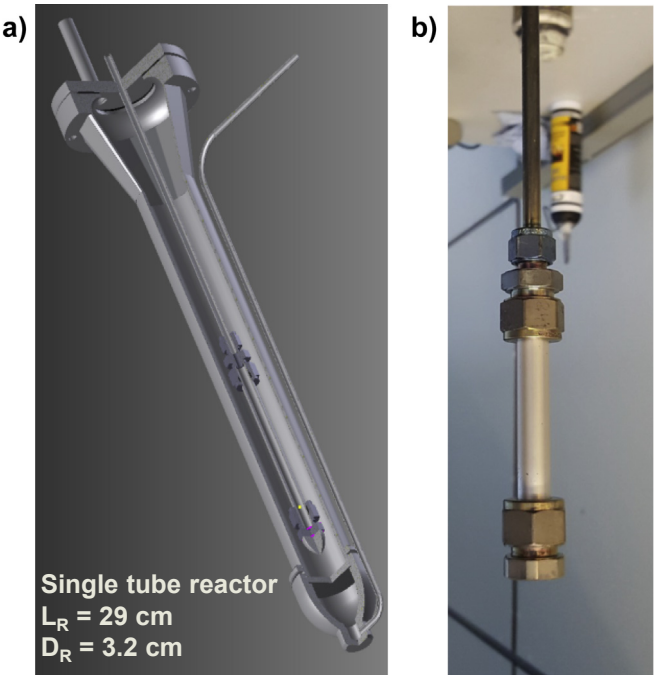

Fig. 3. a) Schematic layout of the single tube membrane reactor; b) Pd-Ag membrane used for the experiments.

The second reactor has an inner diameter of 10 cm and a length of 1 m is located inside an electric heated jacket and details are shown in Fig. 4 and Fig. 5. This experimental set-up allows performing reactive permeation experiments with a maximum of five membranes. There are three thermocouples, and two pressure sensors distributed over the reactor height. A vacuum pump is located at the permeate side, in order to separate H_2 at 10–30 mbar. The system further includes feed connections to pure gas components as O_2, H_2, N_2, CO, CO_2, CH_4 and pressurized air, as well as liquid tanks containing H_2O and EtOH. Both EtOH and water are connected to a CEM (Controlled Evaporator Mixer) where both components can be evaporated before feeding to the reactor. All the tubes connected to the reactor inlet are traced, as well as the tubes used for the retentate, to maintain the temperature well above the boiling point of water and ethanol. In order to measure the EtOH content in the retentate stream, an *Agilent Technologies* Cary 630 FTIR with CaF_2 windows was used together with a *RED-SHIFT* gas sampling system. The FTIR was calibrated prior to the experiments using the classical Lambert-Beer law in typical adsorption spectra for the gases CO_2, CH_4 and EtOH. After that, the retentate passes through a cooler where the water and ethanol (if present) are condensed and separated in a flash column. The retentate is connected to a Sick® analyzer to measure the retentate composition (dry basis). A similar analyzer is also connected to the permeate side, which is able to measure hydrogen concentrations in the range of 0–100% and CO_X concentrations on a ppm level. The flow rate at the permeate side is measured with a Horiba film flow meter. The membranes can also be assessed individually, by closing valves manually which are placed on top of the reactor.

3. Reactor model

The phenomenological two-phase model for the membrane-assisted fluidized bed reactor is depicted in Fig. 6. This model has been developed in the past years and used for different processes involving H_2/O_2 membrane reactors [18,41]. Both emulsion and bubble phases are considered as a cascade of a number of continuous stirred tank reactors (CSTRs) and the size of the CSTRs is directly related to the extent of gas back-mixing in each phase. The model assumptions are as follows: i) the reactor consists of two phases, viz. bubble and emulsion phases; ii) the gas through the emulsion phase is assumed completely mixed in each CSTR and at incipient fluidization conditions; iii) the bubble phase is considered to be in plug flow (and therefore several CSTR are used to properly account for it); iv) the reactions involved in the system occur only in the emulsion phase (i.e. the bubbles are assumed devoid of particles); v) the gas that permeates through the membrane is taken from both bubble and emulsion phases in a ratio according to their local phase fractions; note that the gas extracted from the emulsion phase is replaced by part of the gas transferred from the bubble phase in order to respect the minimum fluidization velocity; vi) the temperature is assumed constant along the entire bed.

The overall component mass balance equations have been formulated accounting for the chemical reactions and the gas permeation in the source terms. More details on the material and energy balances and additional parameters for the membrane-assisted fluidized bed reactor model can be found in Gallucci et al. [32]. (see Table 1)

The kinetic model is based on the results presented by Ruocco

et al. [14], which have been validated against experimental results and compared with other models available in the literature:

- $C_2H_5OH + 3.5\alpha\ O_2 \rightarrow (1-\alpha)C_2H_5OH + 2\alpha CO_2 + 3\alpha H_2O$: the reaction is completely shifted toward the products until the oxygen is completely consumed;
- $(1-\alpha)C_2H_5OH \rightarrow (1-\alpha)CH_4 + (1-\alpha)H_2 + (1-\alpha)CO$: full conversion is assumed with an infinite reaction rate;
- $CH_4 + H_2O \leftrightarrow CO + 3H_2$: the reaction rate of the steam methane reforming (SMR) reaction has been determined experimentally;
- $CO + H_2O \leftrightarrow CO_2 + H_2$: water gas shift reaction (WGS) has been assumed at chemical equilibrium.

An empirical power-law expression is used to describe the kinetics of SMR. The power-law expression generally used for the SMR is:

$$R_{SMR} = k_{SMR}\left(p_{CH_4}^{a} p_{H_2O}^{b} p_{CO}^{c} p_{H_2}^{d}\right)(1-\beta)$$

$$\text{where } \beta = \left(\frac{1}{K_{eq}^{SMR}} \frac{p_{H_2}^{3} p_{CO}}{p_{CH_4} p_{H_2O}}\right) \qquad \begin{matrix} a = 0.96 \\ b = 0.28 \\ c = d = 0 \end{matrix} \qquad (5)$$

$$\text{And } K_{eq}^{SMR} = \exp\left(-\frac{\Delta G^{SMR}}{RT}\right)$$

around 23° can be attributed to amorphous SiO_2 while the diffraction peak at 43.2°, observed in the spectrum of the Pt-Ni/CeO_2-SiO_2 sample, is related to the NiO crystalline phase [44]. Diffraction lines of the CeO_2 fluorite-type structure are also visible in both patterns. As a result of the high surface area of the silica support (400 $m^2\ g^{-1}$), very low dimensions for ceria and nickel oxides crystallites were recorded (equal to 82 and 85 Å respectively). Similarly to the results shown in Table 2, the deposition of the active species had no effect on the ceria crystallite sizes (78 vs 82 Å).

The catalyst was also characterized by H_2-TPR (Fig. 7 (d)) in order to investigate the Ni as well as Pt interactions with the CeO_2/SiO_2 support. Two zones were observed, at 70–200 °C and 200–600 °C, related to the noble and the non-noble metal reduction respectively [45]. Both low and high temperature reduction zones can be deconvoluted into two peaks, which proves the presence of oxides particles with different interactions with the support. In the case of NiO, for example, the peak observed at 294 °C can be ascribed to the reduction of bulk particles, having weak interaction with the support, whereas the peak at 384 °C is attributed to nickel oxide particles in intimate contact with CeO_2/SiO_2. The total hydrogen consumption (3802 $\mu mol_{H2} \cdot g_{cat}^{-1}$) is almost twice the expected one, which suggests that active species deposition on the catalyst may improve the bulk-phase oxygen reduction of CeO_2, commonly negligible below 600 °C [46]. This effect is enhanced by the better Ni reducibility observed after Pt addition,

$$k_{SMR} = k_{0,\,SMR} \exp\left(-\frac{E_{act,\,SMR}}{RT}\right) \qquad \begin{matrix} E_{act,SMR} = 72.8\ kJ/mol \\ k_{0,SMR} = 8.02 \times 10^{-2} mol/(kg_{cat} s\ Pa^{a+b+c+d}) \end{matrix} \qquad (6)$$

related to spillover phenomena and commonly reported in the literature, which also resulted in lower reduction temperatures for nickel oxide phase [47]. On the other hand, the low dimension of

The H_2 permeation rate has been described (mol_{H2}/m^2) with Sieverts' law:

$$J_{H_2} = P_{H_2,0} \exp\left(-\frac{E_{H_2,p}}{RT}\right)\left(p_{H_2,r}^{0.5} - p_{H_2,p}^{0.5}\right) \qquad \begin{matrix} E_{H2,p} = 4.57\ kJ/mol \\ P_{H2,p} = 1.14 \times 10^{-4} mol/(s\ m^2\ Pa^{0.5}) \end{matrix} \qquad (7)$$

The membrane permeation rate is discussed in more detail the next section.

4. Results

4.1. Catalyst characterization

The specific surface area, average pore diameter (D_p) and the pore volume (V_p) of the support and the final catalyst are shown in Table 2. The N_2 adsorption-desorption isotherm curves at 77 K (Fig. 7 (a) and (b)), according to the IUPAC classification, belong to type IV, typical of mesoporous structures [42]. The mesoporous structure of the CeO_2-SiO_2 support as well as its specific area was unaffected by the deposition of the active species. In both cases a broad hysteresis loop was observed, which is typical of mesoporous solids; however, the presence of micropores (pores with sizes smaller than 2 nm) cannot be excluded [43]. The XRD patterns of the support and the catalysts are shown in Fig. 7 (c). The broad peak

ceria crystallites as well as the CeO_2-SiO_2 interactions may further improve ceria surface oxygen reducibility [48].

4.2. Membrane permeation in a single tube reactor

The permeation tests were carried out with the same membrane at the same operating conditions while the reactor configurations were modified. After sealing the membrane (using a torque wrench with a momentum >10 Nm), the membrane leakages are detected by immersing the membrane inside ethanol and feeding He internally to the membrane (with a ΔP of 1 bar). The He leakage is totally concentrated in the sealing part and corresponds to 0.036 ml min^{-1}. After that, the membrane was located inside the reactor and heated up to 400 °C in a N_2 environment. During the heating, air was shortly flowing inside the reactor in order to clean the membrane surface from any unwanted species. When the system is at 400 °C, a mixture of H_2/N_2 is used to activate the membrane. Membrane activation is reached when the H_2

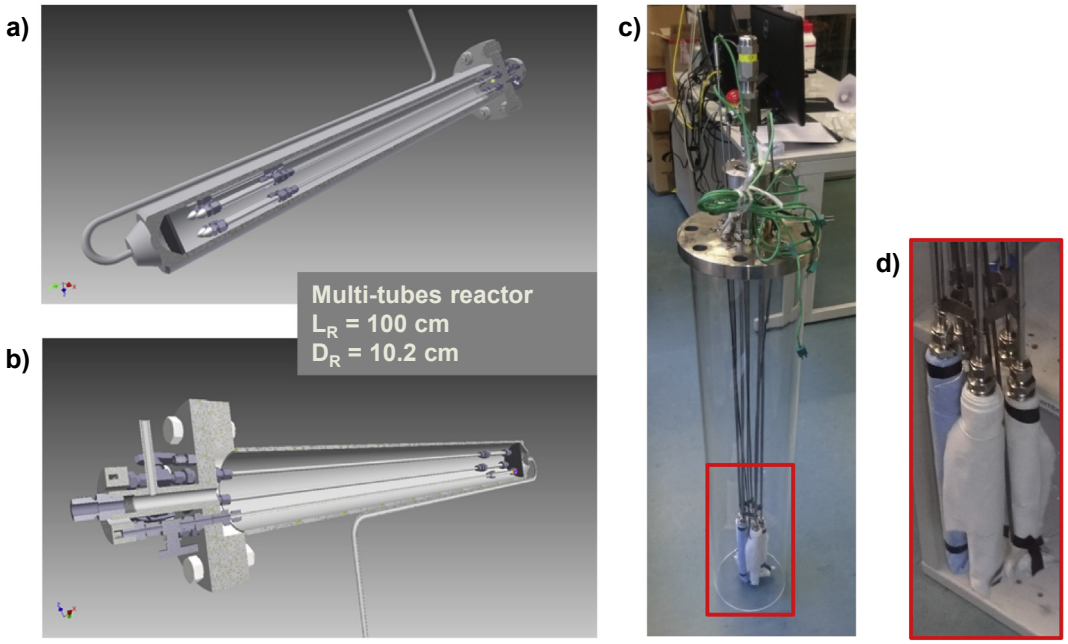

Fig. 4. a) and b) Schematic layout of the multi-tubular membrane reactor; c) membrane tube bank arrangement prior to placement inside the reactor; d) zoomed in picture of the membrane arrangement.

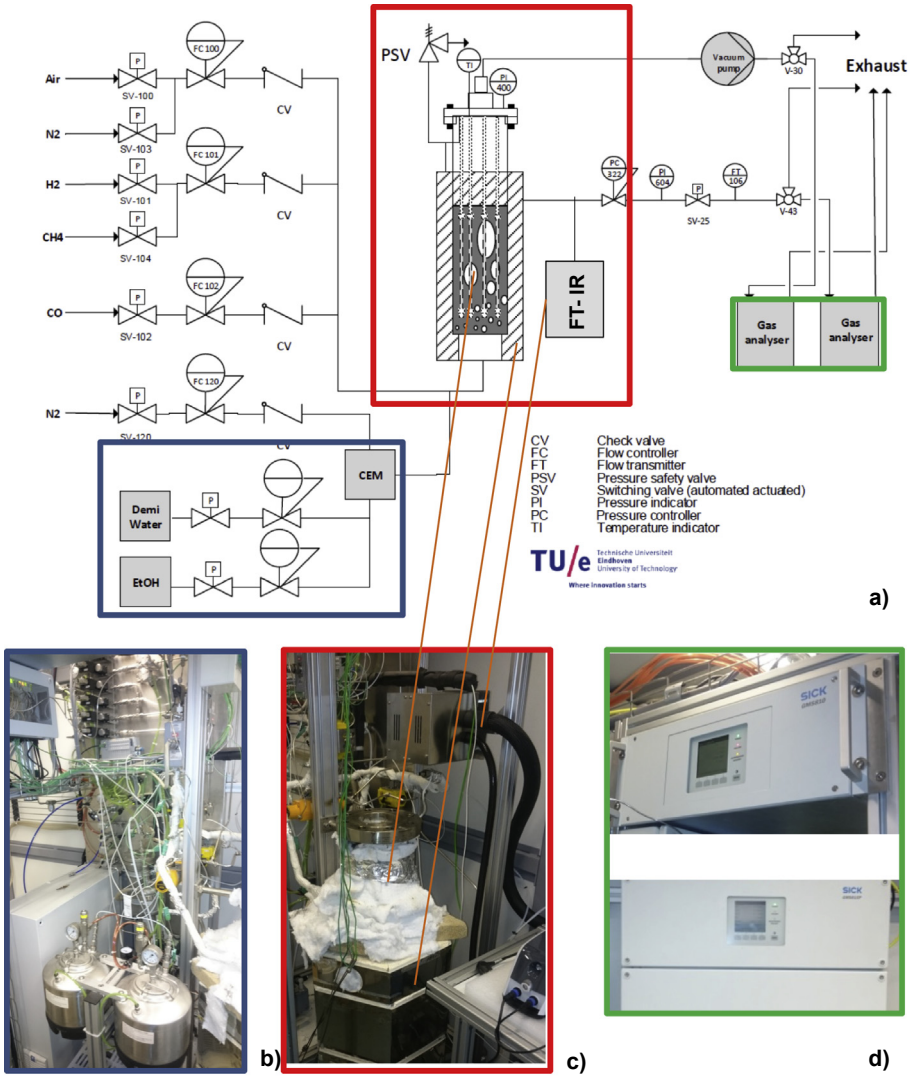

Fig. 5. a) P&ID of the setup used for the multi-tubular experiments; b) Vessels of EtOH and H_2O used for the experiments, c) Electric oven and reactor; d) Gas analysers for the permeate (left) and retentate (right) streams.

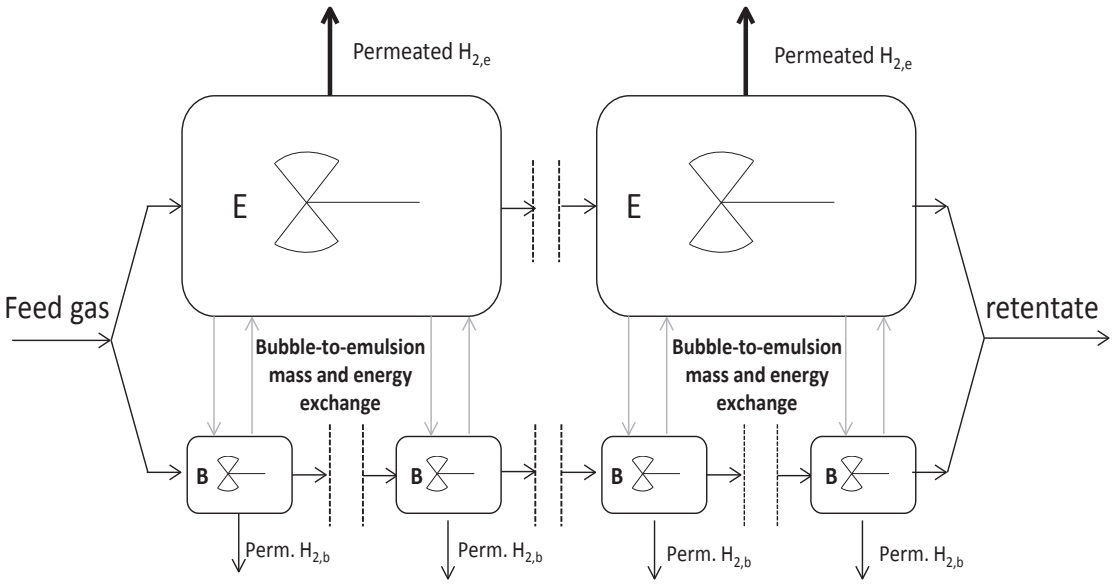

Figure 6. Schematic of the two-phase phenomenological model [32].

permeation is no longer increasing after two consecutive flux measurements.

The first tests have been carried out using the E273 membrane. The membrane permeation rate was measured at 400 °C with three different configurations and the comparison is shown in Fig. 8. In the empty configuration (represented by a circle in Fig. 8), no solids are placed inside the reactor and the permeation tests are carried out using different H_2/N_2 compositions (100/0, 80/20, 60/40, 50/50), where 4 $Nl \cdot min^{-1}$of H_2 is fed to the system while the amount of N_2 is properly adjusted. The total pressure at the feed/retentate side is varied from 1.5 to 4 bar, while the permeate side pressure is kept at 1 bar. Due to limitations in the total pressure, when decreasing the H_2 content fewer measurements were possible in order to guarantee a positive H_2 permeation driving force from the retentate to the permeate side. After the test without solids inside the reactor, two more tests have been carried out. Firstly the reactor has been filled with 95 g of CeO_2/SiO_2 with particle size in the range of 150–250 μm, so that permeation tests could be carried out under fluidization conditions (these results are marked with triangles in Fig. 8). Finally, the reactor has been completely filled with inert material with a particle size of 1–1.5 mm to have the membrane operated in a packed bed configuration (square markers in Fig. 8).

Two main conclusions can be derived from the analysis of these results. The first conclusion is a confirmation that the extent of concentration polarization is considerable. The slope of the curve - which corresponds to the membrane permeance according to equation (7) - decreases by a 53% (respectively $2.18 \cdot 10^{-3}$ mol m^{-2} $s^{-1}Pa^{-0.5}$ and $1.03 \cdot 10^{-3}$ mol m^{-2} $s^{-1}Pa^{-0.5}$) when comparing the gas feed compositions of 100% H_2 and 50/50H_2/N_2. These results are also confirmed by several other works available in the literature [49–53], specifically in the presence of high flux membrane as is the case of ultra-thin (~1 μm thickness) Pd-based membranes. The same trend is also shown in case of fluidized and packed bed configurations. Remarkably, only a negligible improvement (+6–8%) is observed when using the fluidized bed configuration with respect to the packed bed configuration. Helmi et al. [30] have demonstrated that the H_2 permeation in a membrane reactor is enhanced when employing a fluidized bed configuration due to the increased radial dispersion; they have carried out an experimental campaign operating the system at $3 < u/u_{mf} < 5$ by adjusting the flow rate according to the fluidization regime adopted. In this part of the study, the gas flow rate was kept constant resulting in a different fluidization regime. Specifically, when comparing the empty bed with the packed bed configuration, the radial diffusion/dispersion can be estimated at respectively $3.13 \cdot 10^{-4}$ m^2s^{-1} and $1.22 \cdot 10^{-4}$ m^2s^{-1} (according to the Tsotsas and Schlünder [54] correlation) which explains the slightly lower permeation rate obtained with the packed bed configuration. In case of the fluidized bed reactor, when the same inlet flow rate is used, the u/u_{mf} is about 44 ($u_{mf} = 0.014$ ms^{-1}), therefore the gas velocity is almost equal to the terminal velocity u_t estimated at 0.91 m s^{-1}. This implies operation in the slugging regime with the presence of large bubbles surrounding the membrane, which reduces the radial dispersion without any advantages in the permeation rate compared to the empty bed.

4.3. Prototype multi-tubular reactor test

The multi-tubular membrane reactor has been tested in continuous operation. Before starting the permeation test under reactive conditions, the 5 membranes have been checked separately. The results in terms of H_2 permeance[1] and H_2/N_2 ideal perm-selectivity are shown in Table 3, and clearly indicate that the current permselectivity is insufficient to reach the H_2 purity of 99.99% as required for PEM fuel cells applications unless a downstream methanation reactor is used to decrease the CO level in the permeate to values below 10 ppm. However, it should be noted that most of the leakages originates from the sealing of the membrane, thus a stronger support material as well as specific Swagelok connectors could be used to reduce the leakages and improve the permselectivity.

The 5 membranes have been on stream under high temperature and fluidization conditions for three weeks in which reactive experiments (using EtOH) were carried out for overall 50 h. During the remaining time a mixture of N_2 and H_2 was used to keep the bed under fluidization conditions.

The operating temperature of the reactor has been varied in the

[1] The H_2/N_2 ideal perm-selectivity is the average ratio of the H_2 and N_2 permeance values at 450 °C in the range of 2.5–4.5 bar.

Table 1
Hydrodynamic parameters and mass transfer coefficients used in the model.

Parameters	Equation	Ref.
Archimedes number	$Ar = d_p\rho_g\left(\rho_p - \rho_g\right)g/\mu_g$ (8)	[36]
Minimum fluidization velocity	$u_{mf} = \left(\mu_g/d_p\rho_g\right)\left(\sqrt{(27.2)^2 + 0.0408Ar} - 27.2\right)$ (9)	[37]
Bed voidage at minimum fluidization velocity	$\epsilon_{mf} = 0.586Ar^{-0.029}\left(\frac{\rho_g}{\rho_p}\right)^{0.021}$ (10)	[37]
Velocity of rise of swarm of bubbles	$u_b = u_o - u_{mf} + u_{br}$ (11)	[36]
Rising velocity of single bubble	$u_{br} = 0.711\left(g{\cdot}d_{b,avg}\right)^{1/2}$ (12)	[36]
Emulsion velocity	$u_e = \frac{u_o - \delta\cdot u_b}{1 - \delta}$ (13)	[36]
Average bubble diameter	$d_{b,avg} = d_{b,max} - (d_{b,max} - d_{bo})\exp\left(-\frac{0.3H}{D_T}\right)$ (14)	[38]
Initial bubble diameter	$d_{bo} = 0.376\left(u_o - u_{mf}\right)^2$ (15)	[35]
Bubble phase fraction	$\delta_{bn} = \frac{u_b}{u_b}$ (16)	[35]
Emulsion phase fraction	$\delta_{en} = 1 - \delta_{bn}$ (17)	[35]
Maximum superficial bubble gas velocity	$u^s_{b,max} = u_o - u_{mf}$ (18)	[35]
Initial superficial bubble gas velocity	$u^s_{b,o} = u_{br,o}\delta_{bo}$ where $\delta_{bo} = \left(1 - H_{mf}/H_f\right)$ (19)	[35]
Height of bed at minimum fluidization velocity	$H_{mf} = H_s\frac{1 - \epsilon_s}{1 - \epsilon_{mf}}$ (20)	[38]
Height of bed expansion	$H_f = H_{mf}\frac{C_1}{C_1 - C_2}$ (21)	[35]
	where, $C_1 = 1 - \frac{u_{b,o}}{u_{b,avg}}exp\left(-\frac{0.275}{D_T}\right)$ (22)	
	$C_2 = \frac{u_b}{u_{b,avg}}\left[1 - exp\left(-\frac{0.275}{D_T}\right)\right]$ (23)	
Average bubble rise velocity	$u_{b,avg} = u_o - u_{mf} + u_{br}$ (24)	[35]
Gas exchange coefficient	$K_{bc} = 4.5\left(\frac{u_{mf}}{d_p}\right) + 5.85\left(\frac{D_g g^{1/4}}{d_b}\right)$ (25)	[35]
	$K_{ce} = 6.77\left(\frac{D_g\epsilon_{mf}u_b}{d_b}\right)^{1/2}$ (26)	
	$\frac{1}{K_{be}} = \frac{1}{K_{bc}} + \frac{1}{K_{ce}}$ (27)	

Table 2
Physiochemical properties of the fresh CeO_2-SiO_2 and Pt-Ni/CeO_2/SiO_2.

Sample	BET ($m^2 \cdot g^{-1}$)	D_p (nm)	V_p ($cm^3 \cdot g^{-1}$)
CeO_2/SiO_2	254	2.82	0.802
Pt-Ni/CeO_2/SiO_2	255	2.86	0.807

range of 450–550 °C; the pressure at the feed/retentate side has been varied from 2 to 4 bar; the gas flow rate has been adjusted in order to always keep a u/u_{mf} equal to 3. As reference case, the O_2/EtOH ratio has been set at 0.4 (on a molar basis) and the H_2O/EtOH at 6. The amount of EtOH fed to the system has been varied between 100 and 250 $Nml \cdot min^{-1}$ to ensure a constant gas composition and fluidization regime.

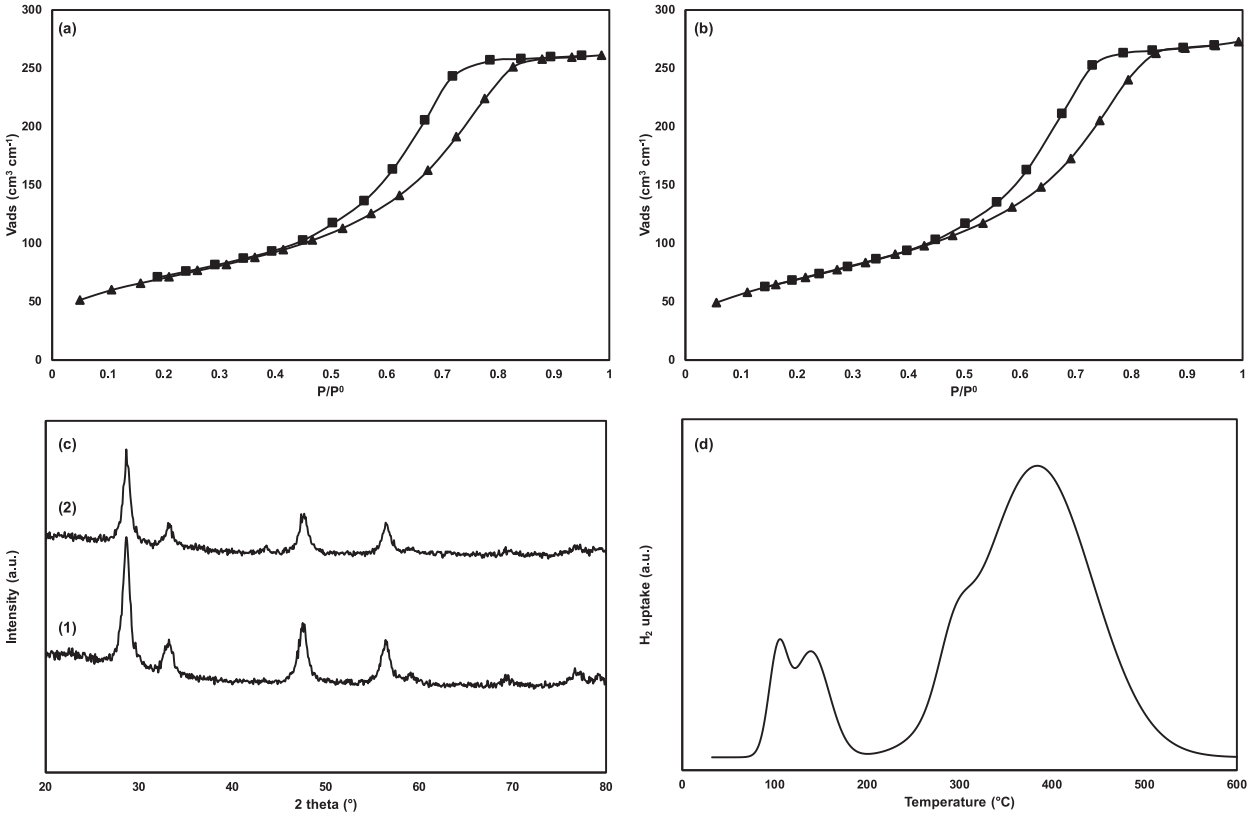

Figure 7. N_2 adsorption (square)-desorption (triangle) isotherms at 77 K for CeO_2/SiO_2 (a) and Pt-Ni/CeO_2/SiO_2 (b), XRD spectra of the support (1) and the final catalyst (2) (c), TPR profile after deconvolution for the Pt-Ni/CeO_2/SiO_2 sample (d).

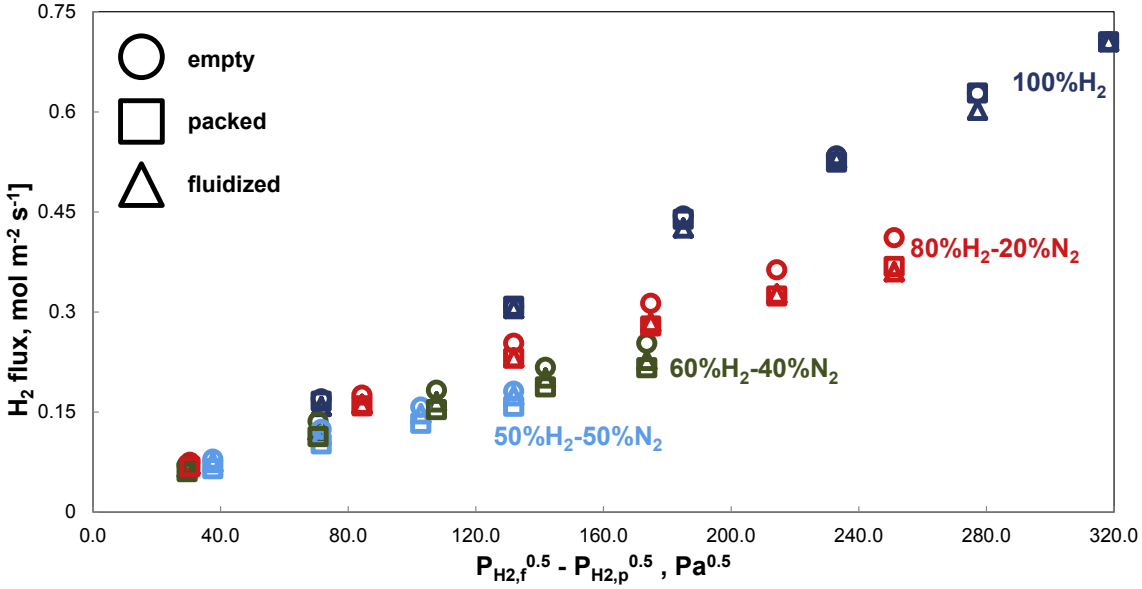

Fig. 8. H_2 flux as a function of the permeation driving force for different H_2-N_2 compositions and configurations at 400 °C with the E273 membrane.

Table 3
Membrane performance used for the prototype before reactive tests.

Membranes	Name	Length	Area	H_2 Permeance (pure gas)	H_2/N_2 Selectivity[Error! Bookmark not defined.]
_	–	mm	cm^2	mol s^{-1} m^{-2} $Pa^{-0.5}$	P_{H2}/P_{N2}
Membr_1	*FL-4*	146.6	47.85	1.46E-03	893
Membr_2	*FL-5*	148.4	48.44	8.58E-04	1319
Membr_3	*FL-6*	175	57.12	8.08E-04	590
Membr_4	*FL-7*	187	61.04	7.36E-04	2836
Membr_5	*FL-8*	153.5	50.10	8.96E-04	803
total area			264.56		

For all the tests, the EtOH conversion at the reactor outlet was above 99.9%, demonstrating that the catalyst was highly active with respect to ESR and EAR reactions and the system is at its thermodynamic equilibrium, when accounting for the hydrogen that has been extracted from the system.

From the analysis of the composition at the retentate side (shown in Fig. 9), the following conclusions can be derived:

- The CH_4 conversion increases when increasing both the temperature or pressure, while the CO content increases at higher temperatures, which confirmes that i) the amount of catalyst and the residence time in the reactor are sufficiently high to avoid any kinetic limitation in the conversion of the reactants and ii) the higher the amount of permeated H_2, the more the

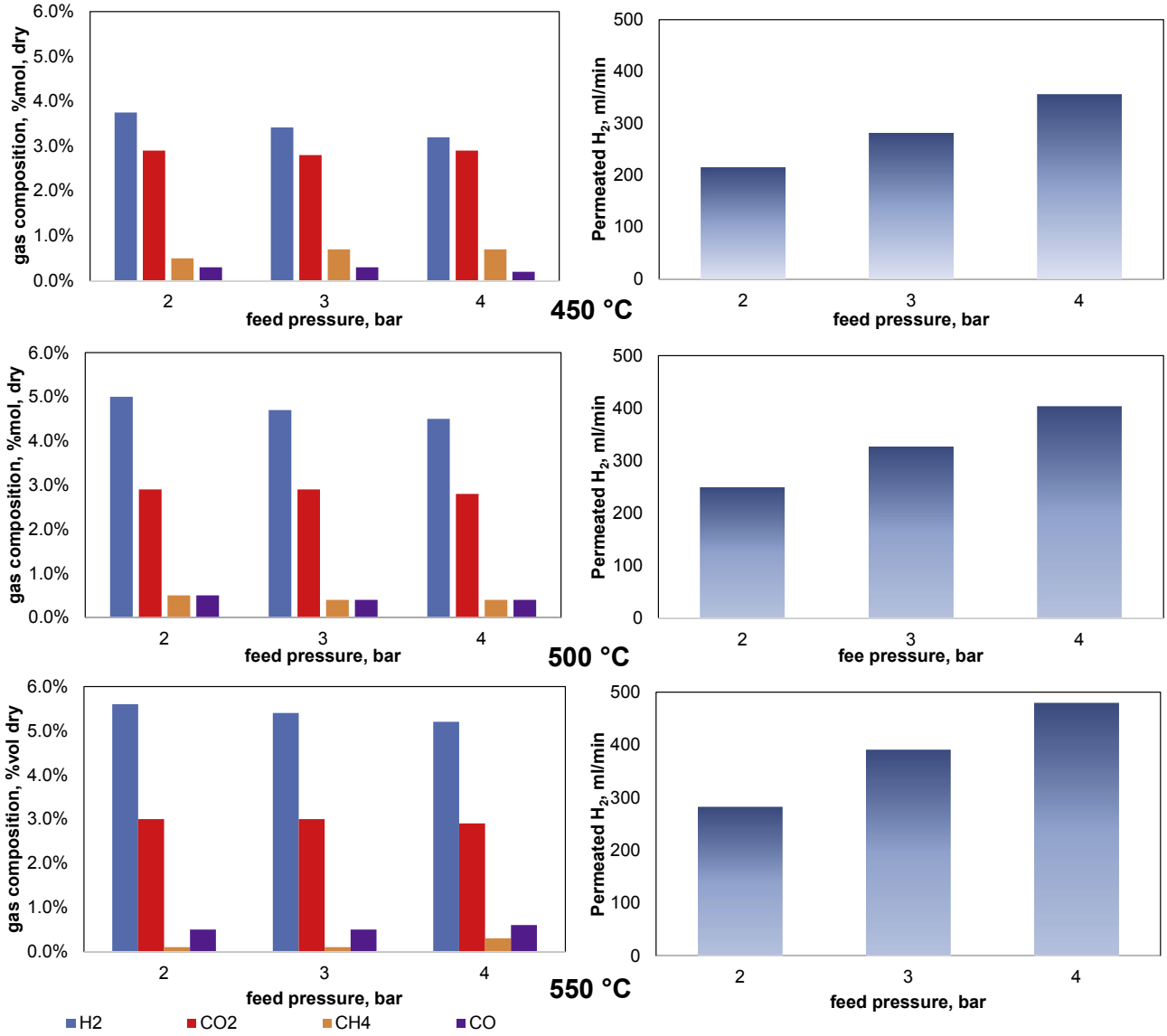

Fig. 9. Results of permeation test at different temperature (450–550 °C) and feed pressure (2–4 bar). The feed composition is EtOH 1.7%, H_2O 10.3%, Air 3.25%, N_2 to balance. The feed flow rate has been varied according to the u/u_{mf}.

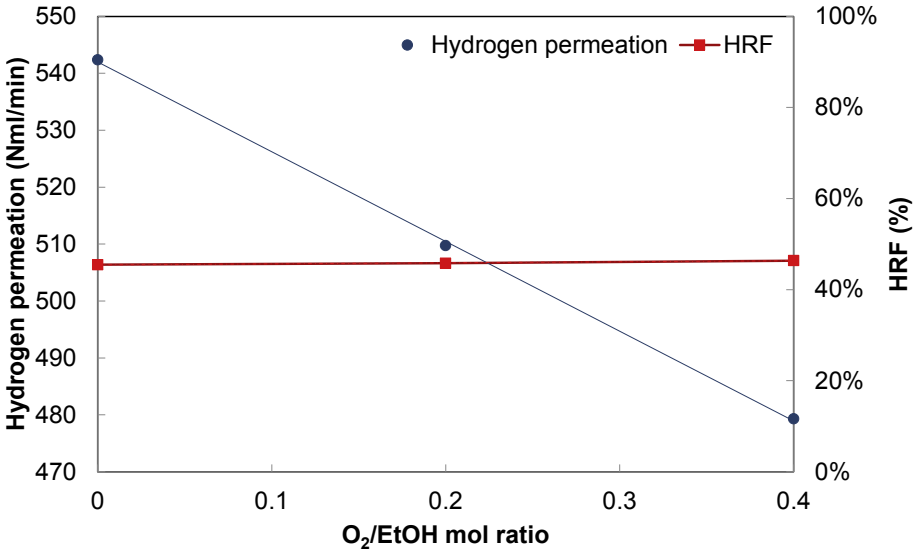

Fig. 10. Effect of the O_2/EtOH ratio on the amount of hydrogen permeated and the hydrogen recovery factor in the EAR membrane reactor.

equilibrium is shifted towards the products. Specifically, at 550 °C the CH_4 fraction is only 0.1–0.3 vol%.

- At increased pressure the amount of H_2 that permeates through the membrane increases due to the higher driving force between the retentate and the permeate side (where 0.03 bar(a) is considered when using the vacuum pump).
- The CO, CO_2, and H_2 concentrations in the permeate side were frequently measured during experiments. The permeated CO and CO_2 concentrations were in the range of 100–300 ppm, whereas the hydrogen concentration was measured constantly at values above 98%, where the remaining 2% is expected to be N_2 for all the experiments.
- The error in the carbon balance is always <5% demonstrating that all the EtOH is converted into CH_4/CO/CO_2 and carbon deposition is not occurring at the investigated conditions.
- With respect to the general definition of the Hydrogen Recovery Factor, HRF[2], the experiments have shown that a higher HRF is reached by increasing the temperature and decreasing the pressure. At a higher pressure the increase in the amount of permeated H_2 is less than the increase in the amount of EtOH fed at the inlet (to achieve the required u/u_{mf}), while at a higher temperature both the increase in the permeation rate and the CH_4 conversion increase the amount of separated H_2. Overall the measured HRF is ranging between 27.5% (@450 °C and 4 bar) to 43% (@ 550 °C and 2 bar).

Decreasing the O_2/EtOH ratio from 0.4 to 0.2 (at 550 °C and 4 bar of feed pressure), the amount of H_2 permeated increases by 6% (from 479 to 509 Nml·min^{-1} of H_2); however, this change does not correspond to an increase in the HRF since the amount of EtOH that react with O_2 is not considered (overall HRF equal to 45.7%). When the system is operated only for the ESR, an thus no oxygen is fed to the system, the permeated H_2 increases up to 542 Nml·min^{-1} (+13%). This behavior can be observed in Fig. 10.

A decrease in the H_2O/EtOH ratio results in a lower H_2 separation (−56%) and consequently in a lower HRF (18.1% vs 46%). As a consequence, the CO and CH_4 content in the retentate stream is increased at the expense of H_2 and CO_2.

A decrease in the u/u_{mf} from 3 to 1.5 results in an increase of the HRF (up to 85%). Despite the amount of gas at the feed side is 50% lower (with the same composition), the amount of permeated H_2 drops from 8% (at O_2/EtOH = 0.4) to 20% (at O_2/EtOH = 0). This demonstrates that in the presence of a larger membrane area, a larger H_2 flow rate can be separated at the permeate side. The experimental campaign had to be stopped after 3 weeks because of a failure in the sealing of four of the membranes.

4.4. Validation of the model

The experimental results were also used for the validation of the reactor model. For the current system, the optimum numbers of CSTRs in series for the emulsion and bubble phases were found to be 6 and 18 respectively. The same number of CSTRs were used also in Gallucci et al. [18] confirming the consistence of the model at a similar fluidization regime. Note that this implies that the bubble phase is indeed in plug flow, and that also the extent of gas backmixing in the emulsion phase is rather small thanks to the compartmentalization via the vertically immersed membrane tube bank.

A comparison of the modelling and experimental results is shown in Fig. 11. The comparison of the retentate composition (at dry and N_2-free conditions) shows a very good agreement between the model and the experimental results, as well as the comparison of the amount of permeated H_2. Additionally, all the experiments described above have been plotted in one single parity plot, in which every gas component is highlighted separately in Fig. 12. The CH_4 and CO results have a somewhat larger error, above 10% (see Fig. 12), which is related due to the relatively high read-off error for these components with the Sick^{TM}-analyzer. From the parity plot it can be concluded that the model with the proposed reaction kinetics, proposed reaction route, and hydrodynamics adequately describes the experimental findings.

Based on the validated model, some analysis has been carried out to compare the effect of kinetics and mass transfer on the final gas conversion at the retentate side and the H_2 production rate. From the computed axial gas composition profiles (Fig. 13), one can conclude that the CO and H_2 mole fractions in the bubble and emulsion phases are very similar. The CH_4 gas fraction differs somewhat more, where the concentration in the bubble phase is

[2] $.HRF = \frac{(H_{2,\ permeated})}{(6C_2H_5OH-2O_2)}$.

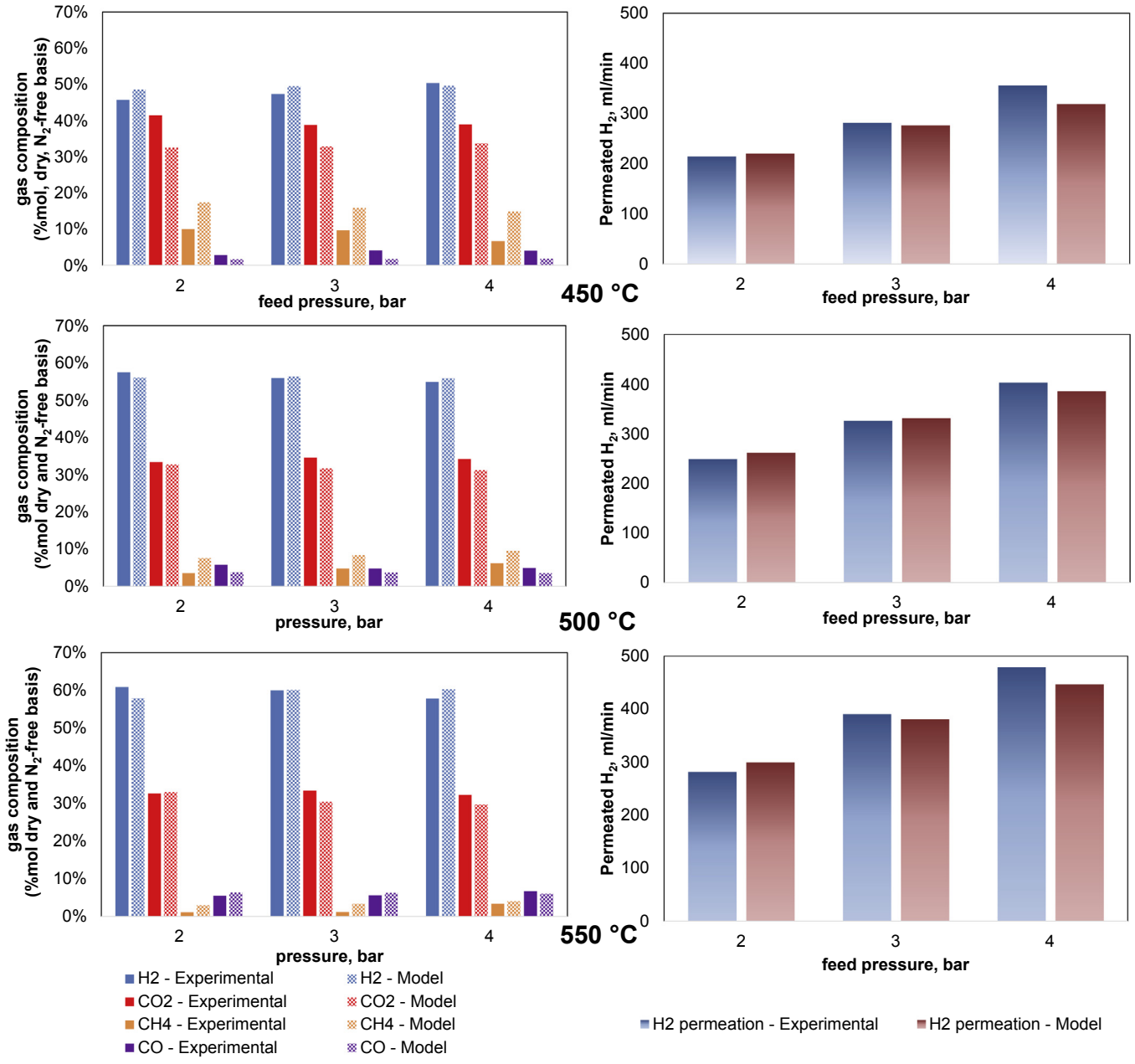

Fig. 11. Comparison of experimental results and model predictions for three different temperatures. Left: retentate composition; right: permeated H_2. The retentate composition is considered after normalization at dry conditions and after removing the amount of N_2.

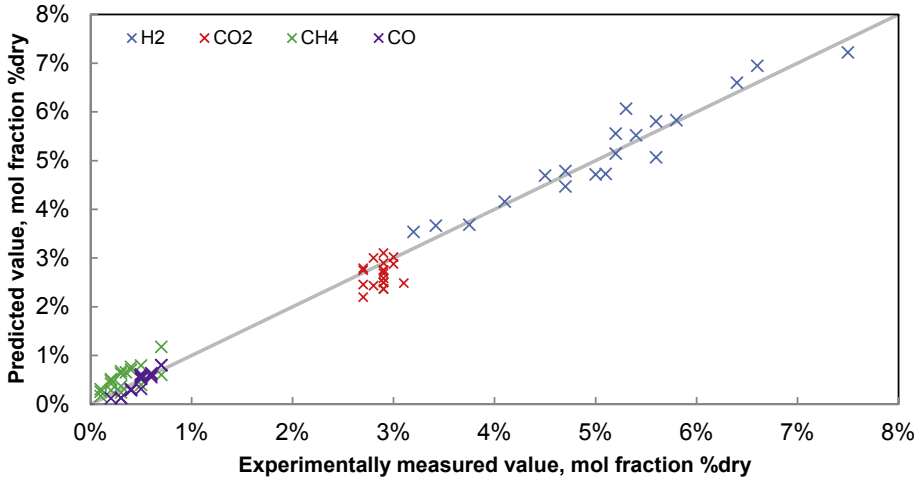

Fig. 12. Parity plot of the results (modelling vs experiments).

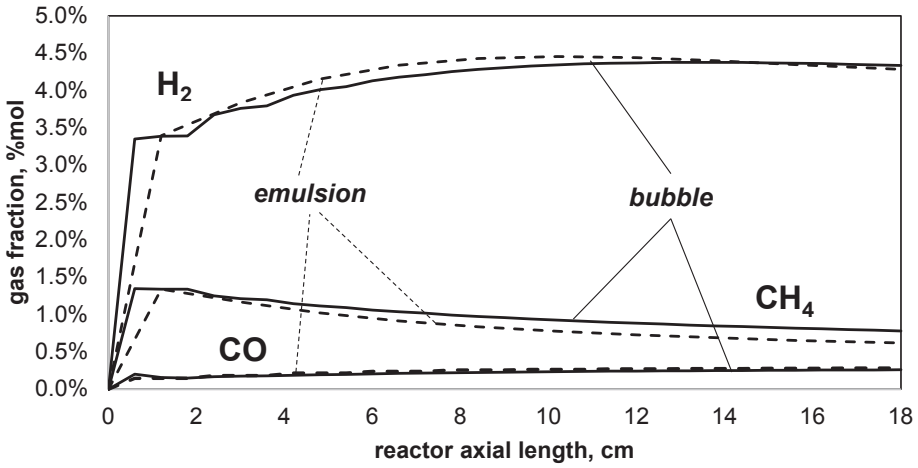

Fig. 13. Axial gas composition profiles (at $T = 500$ °C, $p_{feed} = 4$ bar) for the emulsion and bubble phases.

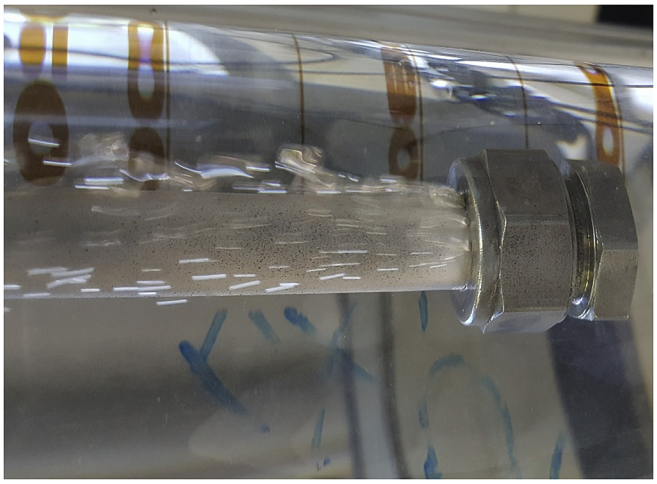

Fig. 14. Leakages from the sealing of the membrane after reactive test during a He leak test.

higher than in the emulsion phase. This can be explained by the higher methane conversion rate by the SMR in the emulsion phase than the CH_4 mass transfer rate from the emulsion to the bubble phase (viz. $0.11 \cdot 10^{-5}$ vs. $0.78 \cdot 10^{-6}$ mol s^{-1}), in particular at the end of the reactor because of the increased bubble size.

After the experimental campaign (approximately 50 h with EtOH, three weeks under H_2/N_2 environment), the membranes were taken out of the reactor and placed in an ethanol solution to perform helium leak test experiments (Fig. 14). One membrane was broken during the shutdown, two of the membranes were leaking mostly from the bottom sealing, while the remaining two membranes were damaged at the upper sealing. This confirms that the sealing of the ceramic–supported membranes is one of the major concerns in this technology that needs to be further developed. Specifically the following recommendations can be made: 1) use of a Swagelok connection with a larger internal diameter (e.g. 12 mm instead of 10 mm); 2) use of predefined graphite ferrules that could avoid the need of any thermal or mechanical pre-treatment, so that no parts of the membrane are in direct contact with the Swagelok where usually the membrane breaks. This also requires an even better accuracy control of the shape of the ceramic supports.

The catalyst particle size distribution was also measured after the experiments and the results indicate that the averaged particle diameter has not changed ($d_{p,av} \approx 190$ μm). However, smaller particles ($d_p < 50$ μm) present in the fresh catalyst were absent. These particles have been blown out of the reactor during the experiments, since the filter to remove particles from the retentate side had to be unblocked a few times.

4.5. Design of FBMR for μCHP unit

The FluidCELL project will demonstrate the feasibility of a FBMR using EtOH as feedstock integrated with a PEM fuel cell up to 5 kW_{el}. This unit is expected to be used for domestic applications to supply electricity and heat. The FBMR is assumed to be operated at 550 °C, 12 bar, 1 bar at the permeate side using H_2O as sweep gas ($H_2O_{sw}/H_{2,p} = 3.7$ kg_{H2O}/kg_{H2}), with at the feed/retentate side a H_2O/EtOH ratio of 3.8 and an (vol.), O_2/EtOH ratio of 0.4 (%vol); The resulting feeding gas mass flow rate is 6.87 kg/h and the composition as calculated from previous work [16] is EtOH 14.9%, H_2O 56.7%, O_2 5.6%, N_2 22.5% (molar basis).

As discussed before, the H_2 content affects the H_2 permeation rate because of the prevailing concentration polarization. Based on the permeation tests a different pre-exponential factor ($\boldsymbol{P_{H2,0}}$) has been adopted in this analysis (Eq. (28)).

$$J_{H_2} = P_{H_2,0} \exp\left(-\frac{E_{H_2,p}}{RT}\right)\left(p_{H_{2,r}}^{0.5} - p_{H_{2,p}}^{0.5}\right) \qquad \begin{matrix} E_{H2,p} = 4.57\ kJ/mol \\ P_{H2,0} = 1.03g10^{-3} mol/(s\ m^2\ Pa^{0.5}) \end{matrix} \tag{28}$$

Since both the kinetics and mass transfer rates do not give rise to any limitation, the membrane area required to separate 3.2 Nm^3/h of H_2 is estimated at 0.44 m^2. Based on this reactor design, the

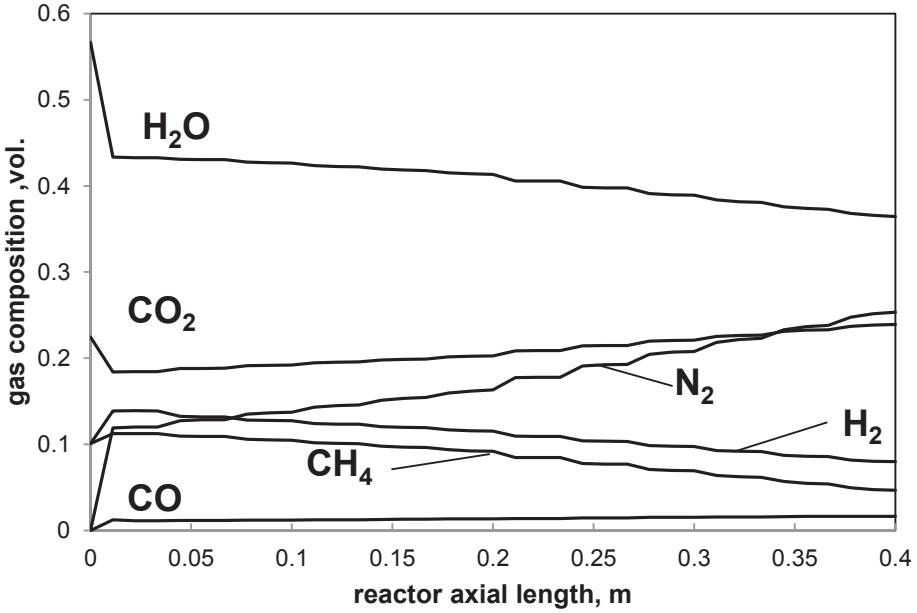

Fig. 15. Axial gas composition profiles at the feed/retentate side.

minimum amount of catalyst needed to keep the retentate at its thermodynamic equilibrium has been calculated. The modelling shows that for a total amount of 7 kg of solid material required to fill the reactor, about 250 g of catalyst is sufficient to achieve the required conversion. In terms of fluidization variables, the minimum u/u_{mf} is ranging from 6 to 9: at the beginning the volumetric flow rate increases because H_2 is produced while consuming CH_4; in the second part of the reactor, the u/u_{mf} decreases because of the larger H_2 permeation rate in comparison with the CH_4 conversion. The computed gas profiles at the feed/retentate are shown in Fig. 15 and the amount of H_2 permeating through the membranes is reported in Fig. 16.

5. Conclusions

The current work has provided an experimental demonstration of a membrane reactor for ethanol auto-thermal reforming together with the validation of a phenomenological model to predict the reactor performance. The integration of EtOH conversion and H_2 separation via thin film Pd-based ceramic supported membranes has been studied and presented. The results of the permeation tests have shown a considerable influence of concentration polarization for the empty, packed and fluidized bed configurations. The three different configurations did not show significant differences in the permeation rate, because the radial diffusion/dispersion rates were comparable for the three considered cases. The permeation tests under reactive conditions have been carried out for more than 50 h (at reactive conditions) and in total 3 weeks under high temperature and fluidization conditions with H_2/N_2, reaching a HRF ranging from 30 to 70% (close to industrial application). The Pt-Ni based catalyst supported on a mixed CeO_2/SiO_2 has demonstrated a high activity and stability for the EAR confirming previous results. The two-phase phenomenological model of a fluidized bed membrane reactor has been described and all its parts including hydrodynamics, mass transfer, kinetics and permeation models were discussed. The validation of the model has been carried out and the model has been subsequently used for the design of a membrane reactor for μCHP applications. For such a configuration 0.44 m^2 of the thin-film supported Pd-based membranes are needed to separate 3.2 $Nm^3 \cdot h_{H2}^{-1}$ using H_2O as sweep gas resulting in an overall HRF of 67% with a substantial reduction in the amount of required catalyst in the fluidized bed (<3.5% wt. basis). These results will be considered for the economic analysis of the system in a future work.

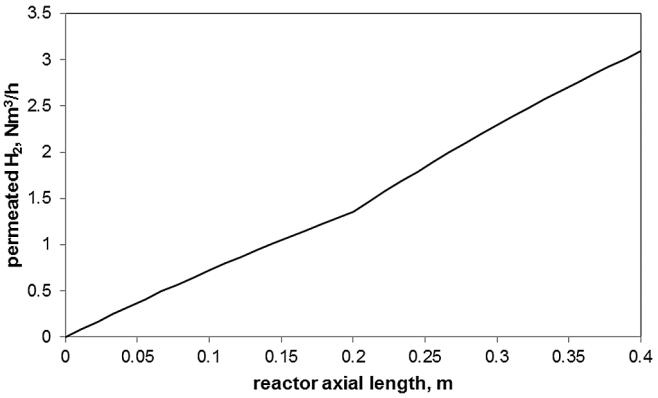

Fig. 16. Volumetric flow rate of H_2 permeated along the reactor length.

Acknowledgements

The presented work is funded within the FluidCELL project as part of the European Union's Seventh Framework Programme (FP7/2007–2013) for the Fuel Cells and Hydrogen Joint Technology Initiative under grant agreement nº 621196.

Nomenclature

ESR	Ethanol Steam Reforming
EAR	Ethanol Auto-Thermal Reforming
WGS	Water Gas Shift
PSA	Pressure Swing Adsorption
CHP	Combined Heat and Power
CEM	Controlled Evaporator Mixer
CSTR	Continuously Stirred Tank Reactor

FBMR	Fluidized Bed Membrane Reactor
HRF	Hydrogen Recovery Factor
PEM	Proton Exchange Membrane
PFR	Plug Flow Reactor
SMR	Steam Methane Reforming

Symbols

Ar	Archimedes Number, [−]
C_i	Concentration of component i, [mol m^{-3}]
C_1, C_2	Coefficient for the bed height expansion, [−]
D_i	Diffusion coefficient of component i, [m^2 s^{-1}]
d_b	Bubble diameter, [m]
d_p	Particle diameter, [m]
d_t	Tube diameter, [m]
E_a	Activation energy, [kJ mol^{-1}]
g	Gravity constant, [m s^{-2}]
H	Bed height, [m]
J	Partial flux, [mol s^{-1}]
K_{eq}	Equilibrium constant, [−]
K_{be}, K_{bc}, K_{ce}	Gas exchange coefficients (bubble −cloud-emulsion phase), [s^{-1}]
k_i	Forward reaction rate constant for reaction i, [mol kg_{cat}^{-1} s^{-1} Pa^{-2}]
$P_{H2,0}$	Permeability of Pd-Ag membrane to H_2, [mol s^{-1} m^{-1} Pa^{-n}]
p_i	Partial pressure of component i, [Pa] or [bar]
R	Gas constant, [J mol^{-1} K^{-1}]
Re	Reynolds number, [−]
Re_{mf}	Reynolds number at minimum fluidization, [−]
r_x	Reaction rate of reaction x, [mol s^{-1}]
M_i	Molecular weight component i, [g mol^{-1}]
S	Selectivity, [−]
T	Temperature, [K]
u_g	Gas velocity, [m s^{-1}]
u_{mf}	Minimum fluidization velocity, [m s^{-1}]
y_i	Molar fraction of component i in gas phase, [−]
φ	Sphericity, [−]
δ	Bubble/emulsion phase fraction, [−]
ε	Porosity, [−]
ε_{mf}	Porosity at minimum fluidization velocity, [−]
μ_i	Viscosity of component i, [kg s^{-1} m^{-1}]
ρ_i	Gas/particle Density, [kg m^{-3}]
K_{ij}	i-phase to j-phase gas exchange coefficient, [s^{-1}]

References

[1] Wawrzinek K, Keller C. Industrial hydrogen production & technology, FuncHy-workshop. 2007. http://www.hzg.de/imperia/md/content/gkss/institut_fuer_werkstoffforschung/wtn/h2-speicher/funchy/funchy-2007/5_linde_wawrzinek_funchy-2007.pdf.

[2] Dunn S. Hydrogen futures: toward a sustainable energy system. Int J Hydrogen Energy 2002;27:235–64. https://doi.org/10.1016/S0360-3199(01)00131-8.

[3] Rostrup-Nielsen T. Manufacture of hydrogen. Catal Today 2005;106:293–6. https://doi.org/10.1016/j.cattod.2005.07.149.

[4] IEA. Technology roadmap hydrogen and fuel cells. 2015. https://doi.org/10.1007/SpringerReference_7300.

[5] Ni M, Leung DYC, Leung MKH. A review on reforming bio-ethanol for hydrogen production. Int J Hydrogen Energy 2007;32:3238–47. https://doi.org/10.1016/j.ijhydene.2007.04.038.

[6] Deluga G a, Salge JR, Schmidt LD, Verykios XE. Renewable hydrogen from ethanol by autothermal reforming. Sci (80-) 2004;303:993–7. https://doi.org/10.1126/science.1093045.

[7] Renewable Fuel Association. 2016 ethanol industry outlook. 2016. http://www.ethanolrfa.org/wp-content/uploads/2016/02/Ethanol-Industry-Outlook-2016.pdf.

[8] Pfromm PH, Amanor-Boadu V, Nelson R, Vadlani P, Madl R. Bio-butanol vs. bio-ethanol: a technical and economic assessment for corn and switchgrass fermented by yeast or Clostridium acetobutylicum. Biomass Bioenergy 2010;34:515–24. https://doi.org/10.1016/j.biombioe.2009.12.017.

[9] Sun S, Yan W, Sun P, Chen J. Thermodynamic analysis of ethanol reforming for hydrogen production. Energy 2012;44:911–24. https://doi.org/10.1016/j.energy.2012.04.059.

[10] De Ávila CN, Hori CE, de Assis AJ. Thermodynamic assessment of hydrogen production and cobalt oxidation susceptibility under ethanol reforming conditions. Energy 2011;36:4385–95. https://doi.org/10.1016/j.energy.2011.04.004.

[11] Hou T, Zhang S, Chen Y, Wang D, Cai W. Hydrogen production from ethanol reforming: catalysts and reaction mechanism. Renew Sustain Energy Rev 2015;44:132–48. https://doi.org/10.1016/j.rser.2014.12.023.

[12] Haryanto A, Fernando S, Murali N, Adhikari S. Current status of hydrogen production techniques by steam reforming of ethanol: a review. Energy Fuels 2005:2098–106.

[13] Palma V, Castaldo F, Ciambelli P, Iaquaniello G. CeO2-supported Pt/Ni catalyst for the renewable and clean H2 production via ethanol steam reforming. Appl Catal B Environ 2014;145:73–84. https://doi.org/10.1016/j.apcatb.2013.01.053.

[14] Ruocco C, Meloni E, Palma V, van Sint Annaland M, Spallina V, Gallucci F. Pt–Ni based catalyst for ethanol reforming in a fluidized bed membrane reactor. Int J Hydrogen Energy 2016;41:20122–36. https://doi.org/10.1016/j.ijhydene.2016.08.045.

[15] Palma V, Ruocco C, Meloni E, Ricca A. Oxidative steam reforming of ethanol on mesoporous silica supported PtNi/CeO2 catalysts. Int J Hydrogen Energy 2016;42:1598–608. https://doi.org/10.1016/j.ijhydene.2016.05.071.

[16] Foresti S, Manzolini G. Performances of a micro-CHP system fed with bio-ethanol based on fluidized bed membrane reactor and PEM fuel cells. Int J Hydrogen Energy 2016;41:9004–21. https://doi.org/10.1016/j.ijhydene.2016.03.210.

[17] Galletti C, Specchia S, Saracco G, Specchia V. CO-selective methanation over Ru–γAl2O3 catalysts in H2-rich gas for PEM FC applications. Chem Eng Sci 2010;65:590–6. https://doi.org/10.1016/j.ces.2009.06.052.

[18] Gallucci F, van Sint Annaland M, Kuipers J. Autothermal reforming of methane with integrated CO2 capture in a novel fluidized bed membrane reactor. Part 2 comparison of reactor configurations. Top Catal 2008;51:146–57. https://doi.org/10.1007/s11244-008-9127-7.

[19] Borgognoni F, Tosti S, Vadrucci M, Santucci A. Combined methane and ethanol reforming for pure hydrogen production through Pd-based membranes. Int J Hydrogen Energy 2013;38:1430–8. https://doi.org/10.1016/j.ijhydene.2012.11.036.

[20] Basile A, Gallucci F, Iulianelli A, Tosti S. CO-free hydrogen production by ethanol steam reforming in a Pd-Ag membrane reactor. Fuel Cells 2008;8:62–8. https://doi.org/10.1002/fuce.200700018.

[21] Hedayati A, Le Corre O, Lacarrière B, Llorca J. Dynamic simulation of pure hydrogen production via ethanol steam reforming in a catalytic membrane reactor. Energy 2016;117:316–24. https://doi.org/10.1016/j.energy.2016.06.042.

[22] Sjardin M, Damen KJ, Faaij APC. Techno-economic prospects of small-scale membrane reactors in a future hydrogen-fuelled transportation sector. Energy 2006;31:2187–219. https://doi.org/10.1016/j.energy.2005.12.004.

[23] Jian Q, Zhao Y, Wang H. An experimental study of the dynamic behavior of a 2 kW proton exchange membrane fuel cell stack under various loading conditions. Energy 2015;80:740–5. https://doi.org/10.1016/j.energy.2014.12.032.

[24] Fernandez E, Sanchez-Garcia JA, Melendez J, Spallina V, van Sint Annaland M, Gallucci F, et al. Development of highly permeable ultra-thin Pd-based supported membranes. Chem Eng J 2016;305:149–55. https://doi.org/10.1016/j.cej.2015.11.060.

[25] Acha E, Requies J, Barrio VL, Cambra JF, Güemez MB, Arias PL, et al. PdCu membrane applied to hydrogen production from methane. J Memb Sci 2012;415–416:66–74. https://doi.org/10.1016/j.memsci.2012.04.038.

[26] Sarić M, Van Delft YC, Sumbharaju R, Meyer DF, De Groot A. Steam reforming of methane in a bench-scale membrane reactor at realistic working conditions. Catal Today 2012;193:74–80. https://doi.org/10.1016/j.cattod.2012.04.009.

[27] Vicinanza N, Svenum IH, Næss LN, Peters TA, Bredesen R, Borg A, et al. Thickness dependent effects of solubility and surface phenomena on the hydrogen transport properties of sputtered Pd77%Ag23% thin film membranes. J Memb Sci 2015;476:602–8. https://doi.org/10.1016/j.memsci.2014.11.031.

[28] Medrano JA, Fernandez E, Melendez J, Parco M, Tanaka DAP, Van Sint Annaland M, et al. Pd-based metallic supported membranes: high-temperature stability and fluidized bed reactor testing. Int J Hydrogen Energy 2016;41:8706–18. https://doi.org/10.1016/j.ijhydene.2015.10.094.

[29] Hwang KR, Park JW, Lee SW, Hong S, Lee CB, Oh DK, et al. Catalytic combustion of the retentate gas from a CO2/H2 separation membrane reactor for further CO2 enrichment and energy recovery. Energy 2015;90:1192–8. https://doi.org/10.1016/j.energy.2015.06.067.

[30] Helmi A, Fernandez E, Melendez J, Tanaka DAP, Gallucci F, Van Sint Annaland M. Fluidized bed membrane reactors for ultra pure H2 production - a step forward towards commercialization. Molecules 2016;21. https://doi.org/10.3390/molecules21030376.

[31] Brunetti A, Caravella A, Fernandez E, Tanaka DA Pacheco, Gallucci F, Drioli E, et al. Syngas upgrading in a membrane reactor with thin Pd-alloy supported membrane. Int J Hydrogen Energy 2015;40:10883–93. https://doi.org/10.1016/j.ijhydene.2015.07.002.

[32] Gallucci F, Van Sint Annaland M, Kuipers JAM. Pure hydrogen production via

autothermal reforming of ethanol in a fluidized bed membrane reactor: a simulation study. Int J Hydrogen Energy 2010;35:1659–68. https://doi.org/10.1016/j.ijhydene.2009.12.014.
[33] De Falco M. Ethanol membrane reformer and PEMFC system for automotive application. Fuel 2011;90:739–47. https://doi.org/10.1016/j.fuel.2010.09.054.
[34] Arratibel Plazaola A, Tanaka D Pacheco, Van Sint Annaland M, Gallucci F. Recent advances in Pd-Based membranes for membrane reactors. Molecules 2017;22:51. https://doi.org/10.3390/molecules22010051.
[35] Maurer S, Wagner EC, Schildhauer TJ, van Ommen JR, Biollaz SMA, Mudde RF. X-ray measurements of bubble hold-up in fluidized beds with and without vertical internals. Int J Multiph Flow 2015;74:118–24. https://doi.org/10.1016/j.ijmultiphaseflow.2015.03.009.
[36] Dang TYN, Gallucci F, Van Sint Annaland M. Gas back-mixing study in a membrane-assisted micro-structured fluidized bed. Chem Eng Sci 2014;108:194–202. https://doi.org/10.1016/j.ces.2014.01.013.
[37] Dang NTY, Gallucci F, Van Sint Annaland M. Micro-structured fluidized bed membrane reactors: solids circulation and densified zones distribution. Chem Eng J 2014;239:42–52. https://doi.org/10.1016/j.cej.2013.11.001.
[38] Tanaka DA Pacheco, Llosa Tanco MA, Niwa SI, Wakui Y, Mizukami F, Namba T, et al. Preparation of palladium and silver alloy membrane on a porous??-alumina tube via simultaneous electroless plating. J Memb Sci 2005;247:21–7. https://doi.org/10.1016/j.memsci.2004.06.002.
[39] Chen W, Hu X, Wang R, Huang Y. On the assembling of Pd/ceramic composite membranes for hydrogen separation. Sep Purif Technol 2010;72:92–7. https://doi.org/10.1016/j.seppur.2010.01.010.
[40] Fernandez E, Coenen K, Helmi A, Melendez J, Zuñiga J, Tanaka DA Pacheco, et al. Preparation and characterization of thin-film Pd-Ag supported membranes for high-temperature applications. Int J Hydrogen Energy 2015;40:13463–78. https://doi.org/10.1016/j.ijhydene.2015.08.050.
[41] Gallucci F, Annaland M, Kuipers J. Autothermal reforming of methane with integrated CO2 capture in a novel fluidized bed membrane reactor. Part 1: experimental demonstration. Top Catal 2008;51:133–45. https://doi.org/10.1007/s11244-008-9126-8.
[42] Carmody O, Frost R, Xi Y, Kokot S. Surface characterisation of selected sorbent materials for common hydrocarbon fuels. Surf Sci 2007;601:2066–76. https://doi.org/10.1016/j.susc.2007.03.004.
[43] Zhang Q, Zhang T, Shi Y, Zhao B, Wang M, Liu Q, et al. A sintering and carbon-resistant Ni-SBA-15 catalyst prepared by solid-state grinding method for dry reforming of methane. J CO2 Util 2017;17:10–9. https://doi.org/10.1016/j.jcou.2016.11.002.
[44] Kang S, Sub Kwak B, Kang M. Synthesis of Ni-alkaline earth metals particles encapsulated by porous SiO2 (NiMO@SiO2) and their catalytic performances on ethanol steam reforming. Ceram Int 2014;40:14197–206. https://doi.org/10.1016/j.ceramint.2014.06.008.
[45] Palma V, Ruocco C, Ricca A. Ceramic foams coated with PtNi/CeO2ZrO2 for bioethanol steam reforming. Int J Hydrogen Energy 2016;41:11526–36. https://doi.org/10.1016/j.ijhydene.2016.04.028.
[46] Palma V, Ruocco C, Meloni E, Ricca A. Coke-resistant Pt-Ni/CeO 2 -SiO 2 catalysts for ethanol reforming 2017;57:1675–80. https://doi.org/10.3303/CET1757280.
[47] Li D, Nishida K, Zhan Y, Shishido T, Oumi Y, Sano T, et al. Superior catalytic behavior of trace Pt-doped Ni/Mg(Al)O in methane reforming under daily start-up and shut-down operation. Appl Catal A Gen 2008;350:225–36. https://doi.org/10.1016/j.apcata.2008.08.017.
[48] da Silva AGM, Fajardo HV, Balzer R, Probst LFD, Prado NT, Camargo PHC, et al. Efficient ceria–silica catalysts for BTX oxidation: probing the catalytic performance and oxygen storage. Chem Eng J 2016;286:369–76. https://doi.org/10.1016/j.cej.2015.10.097.
[49] Zhang J, Liu D, He M, Xu H, Li W. Experimental and simulation studies on concentration polarization in H 2 enrichment by highly permeable and selective Pd membranes. J Memb Sci 2006;274:83–91. https://doi.org/10.1016/j.memsci.2005.07.047.
[50] Nakajima T, Kume T, Ikeda Y, Shiraki M, Kurokawa H, Iseki T, et al. Effect of concentration polarization on hydrogen production performance of ceramic-supported Pd membrane module. Int J Hydrogen Energy 2015;40:11451–6. https://doi.org/10.1016/j.ijhydene.2015.03.088.
[51] Hara S, Sakaki K, Itoh N. Decline in hydrogen permeation due to concentration polarization and CO hindrance in a palladium membrane reactor. Ind Eng Chem Res 1999;38:4913–8. https://doi.org/10.1021/ie990200n.
[52] Caravella A, Melone L, Sun Y, Brunetti A, Drioli E, Barbieri G. Concentration polarization distribution along Pd-based membrane reactors: a modelling approach applied to Water-Gas Shift. Int J Hydrogen Energy 2016;41:2660–70. https://doi.org/10.1016/j.ijhydene.2015.12.141.
[53] Fernandez E, Helmi A, Coenen K, Melendez J, Viviente JL, Tanaka DA Pacheco, et al. Development of thin Pd–Ag supported membranes for fluidized bed membrane reactors including WGS related gases. Int J Hydrogen Energy 2015;40:3506–19. https://doi.org/10.1016/j.ijhydene.2014.08.074.
[54] Tsotsas E, Schlünder EU. Heat transfer in packed beds with fluid flow: remarks on the meaning and the calculation of a heat transfer coefficient at the wall. Chem Eng Sci 1990;45:819–37. https://doi.org/10.1016/0009-2509(90)85005-X.